Research Article

Yao Chen, Aiqin Wang*, Zishuo Guo, and Jingpei Xie

Molecular dynamics study of deformation mechanism of interfacial microzone of $Cu/Al_2Cu/Al$ composites under tension

https://doi.org/10.1515/ntrev-2022-0072
received July 7, 2021; accepted February 17, 2022

Abstract: The micromechanical behavior of an $Al/Al_2Cu/Cu$ multilayer with characteristic crystal orientation during uniaxial tensile deformation was investigated by molecular dynamics. The simulation results showed that under tensile loading, the dislocation nucleates at the Cu/Al_2Cu heterogeneous interface and moves toward the Cu layer along the {111} crystal plane. The deformation mechanism is intralayer confinement slip. As the dislocations proliferated, interactions between them occurred; resulting in the formation of insertion stacking faults and deformation twins in the Cu and Al layers. However, no dislocation lines were generated in the Al_2Cu layer during tensile deformation. As the load increased, the stress concentration at the Al_2Cu/Al interface led to the fracture of the complex. In addition, the microplastic deformation mechanism and mechanical properties of $Al/Al_2Cu/Cu$ composites at different temperatures and strain rates were significantly different. These results revealed the microdeformation mechanism of laminated composites containing brittle phases.

Keywords: molecular dynamics simulation, tensile loading, plastic deformation mechanism

1 Introduction

A Cu/Al composite board [1–4] combines the low resistance and high thermal conductivity of copper with the lightweight and low price of aluminum to balance the price/performance combination of copper and aluminum. Its weight can be reduced by 35–50%, and its thermal and electrical conductivity is comparable to some copper alloys. Electrical power, heat, electronics, communications, new energy photovoltaics, and transportation all benefit from this combination. Using aluminum instead of copper reduces the amount of copper used, which contributes to the more efficient use of resources [5,6].

As a composite material with a multi-scaled configuration, the Cu/Al layered composite material has mechanical and physical properties closely related to the interface structure and preparation process [7–9]. There are differences in the initial state of the component layer raw materials used in different preparation methods, resulting in differences in the interface structure and microstructure of the composite board component layer obtained by different preparation methods, and the component layer microstructure evolves differently during annealing, resulting in large differences in the strength and plasticity of annealed composites with different preparation methods. Kim and Hong [7] studied the tensile deformation of Cu/Al/Cu layered composites. This study found that the composites' tensile strength exceeded that of the law of mixing while examining the interaction between interactive deformation and composite toughness. Due to the constraints of the strong bonding interface, the interactive deformation of the copper layer and the aluminum layer beneficially improved the ductility of the Cu/Al composite. Liu *et al.* [8,9] prepared layered Cu/Al composites by casting-rolling. They found that in the cast-rolled state, the copper–aluminum composite plate produced a tougher composite. Through analysis of the microstructure evolution and the interface fracture behavior during the deformation of the tensile specimen, they initially believed that toughening

* **Corresponding author: Aiqin Wang,** School of Materials Science and Engineering, Henan University of Science and Technology, Luoyang 471023, China, e-mail: aiqin_wang888@163.com
Yao Chen, Zishuo Guo: School of Materials Science and Engineering, Henan University of Science and Technology, Luoyang 471023, China
Jingpei Xie: School of Materials Science and Engineering, Henan University of Science and Technology, Luoyang 471023, China; Collaborative Innovation Centers of Non-Ferrous Materials of Henan Province, Luoyang 471023, China

in the Cu/Al composite plate was caused by the coordinated deformation of the composite plate. At the same time, studies have found that during the preparation or diffusion annealing of copper/aluminum composite panels, micro/nano level multilayer intermetallic compounds formed at the interface, such as Al_2Cu and Al_4Cu_9 [10–12]. The presence of hard and brittle intermetallic compounds leads to composite material fractures at the interface layer. This makes the interface problem a core issue in the study of copper–aluminum composite materials.

Molecular dynamics simulations can reveal the dynamic deformation behavior of interfacial microdomains at the atomic scale. Recently, many studies have simulated the interfacial microdomains in laminated composites. Rezaei [13] used molecular dynamics to study the tensile properties of graphene/copper nanocomposites under different strains and found the graphene layer not only increased the strength and yield strain of the material but also increased the stiffness and plasticity of the material. Yang *et al.* [14] studied the deformation mechanism of semi-coherent interfaces under compression loading, and their results showed a semi-coherent interface formed during dislocations and simultaneously hindered their propagation, which improved the strength and plasticity of the alloy under compression loading. Zhou *et al.* [15] studied the mechanical properties of nano-Cu/Al multilayer films and found that its strength reached 7.7 GPa. A molecular dynamics analysis showed that twins and stacking faults were the main mechanisms of hardness enhancement. Especially when $h < 5$ nm, stable stacking faults at the Cu/Al layer interface dominate. Weng *et al.* [16] used molecular dynamics to analyze the deformation of graphene/Cu composites under compressive load. Graphene plays a role in load transfer and hinders dislocation movements. At the same time, as the core of dislocation nucleation, graphene improves the plastic deformation ability of composite materials.

This work examined the nano-multilayered Cu/Al composite containing the brittle phase Al_2Cu. By conducting molecular dynamics simulations of uniaxial stretching, the microscopic configuration of various deformations at the heterogeneous interface was activated on the atomic scale. The effects of temperature and strain rate on the tensile deformation of the system were studied in detail. These results contribute to a better understanding of the microphysical process of plastic deformation in Cu/Al multilayer composites and provide theoretical guidance for the design and use of Cu/Al layered composites.

Table 1: Crystal structures of Cu, Al and Al_2Cu

Element name	Crystal structure	Space group	Lattice parameters (nm)
Cu	fcc	$Fm\text{-}3\bar{3}m$	$a = b = c = 0.3615$
Al	fcc	$Fm\text{-}3\bar{3}m$	$a = b = c = 0.4049$
Al_2Cu	Tetragonal	$I4/mcm$	$a = b = 0.6067$; $c = 0.4877$

2 Computational models and methods

The Cu–Al interfacial system consists of Cu, Al, and Al_2Cu. Their crystal structures are shown in Table 1 [17]. The micromechanical behavior of Al/Al_2Cu/Cu layered composites during uniaxial tensile deformation was simulated by molecular dynamics. The multi-layer complex model of the sandwich structure is shown in Figure 1. The metal layers of the model from top to bottom are Cu, Al_2Cu, and Al.

2.1 Uniaxial tensile model

The uniaxial tensile model is a four-prism, as shown in Figure 1. The *X* and *Y*-axis directions in the model represent free boundary conditions. The *x*-direction was [$1\bar{2}1$] Cu//[001]Al_2Cu//[$1\bar{2}1$]Al, with a specific atomic layer size of 11 nm in the corresponding direction, proportional to 27 periodic Cu unit cells, 25 periodic Al_2Cu unit cells, and 24 periodic Al unit cells, while the *y*-direction was [$10\bar{1}$]

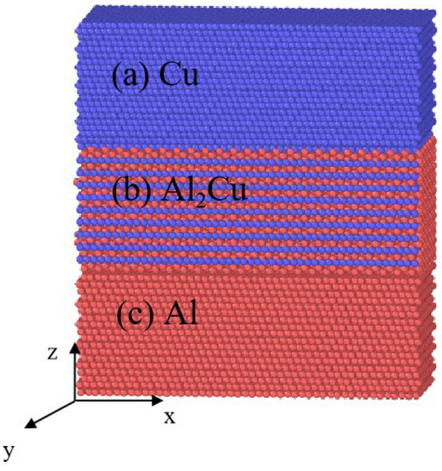

Figure 1: Cu/Al_2Cu/Al multilayer structure: (a) Cu; (b) Al_2Cu; (c) Al.

Table 2: The initial orientation of Cu, Al and Al_2Cu layers

Layer	Axis		
	X	*Y*	*Z*
Cu	$[1\bar{2}1]$	$[10\bar{1}]$	[111]
Al	$[1\bar{2}1]$	$[10\bar{1}]$	[111]
Al_2Cu	[001]	[110]	$[\bar{1}10]$

Cu//[110]Al_2Cu//$[10\bar{1}]$Al, with specific atomic layer size of 5 nm in the corresponding direction, proportional to 10 periodic Cu unit cells, six periodic Al_2Cu units cell and nine periodic Al unit cells. The length of the *X*, *Y*, and *Z*-axis was approximately 11, 5, and 12 nm, respectively. The uniaxial tensile deformation of the complex was realized by applying the periodic boundary conditions of the strain along the *Z*-axis. The total number of atoms in the model was 54,432. The strain rate was 10^{10} s^{-1}. The target shape variable of uniaxial tensile deformation was $\varepsilon = 0.4$. Table 2 shows the initial crystal orientations of the Cu, Al, and Al_2Cu layers [18–20].

In the complex model, the interatomic interactions of Cu–Cu, Al–Al, and Cu–Al used a bond order potential [21]. The time step of the simulation process was 0.001 ps. The model was initially relaxed for 50 ps under an isothermal and isobaric (NPT) ensemble, so the model temperature stabilized at 300 K, and the energy was minimized. Then, the model was subjected to uniaxial tensile deformation. Simulation results were obtained using the Open Visualization Tool (OVITO) software, and the results of the microstructure analysis were completed based on the Discontinuities Extraction Algorithm (DXA). Atoms of FCC, HCP, BCC, and unknown structural types are shown in green, red, blue, and white, respectively.

3 Results and discussion

The stress–strain curve of the vertical interface tensile deformation is shown in Figure 2. On the stress–strain curve, there are two stages of deformation. In the first stage of stretching, the material initially undergoes elastic deformation with an almost linear stress–strain curve (section AB). When the strain increases to 0.068 (point B), the material enters the yield stage with an initial yield strength of 7.23 GPa. When the strain increases to 0.085, the stress maximizes (point D) and decreases sharply with the onset of plastic deformation. Deformation in the second stage, the curve of the fluctuations in

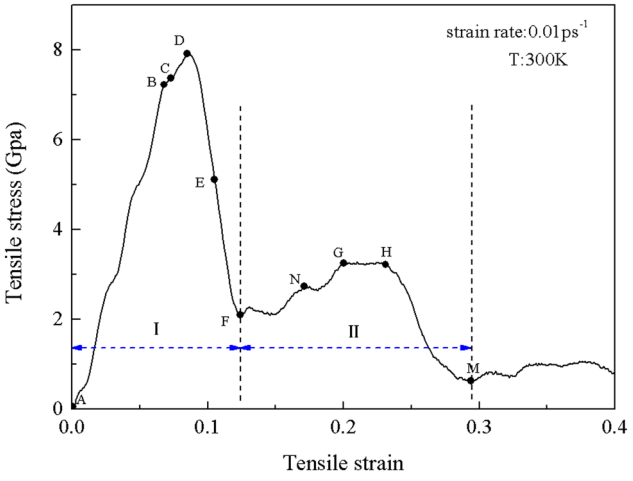

Figure 2: Stress–strain curve of $Cu/Al_2Cu/Al$ interface system under vertical interface tensile load.

the growth stage (Section FG) appears as a twofold yield, with increases in strain, and stress begins to rise again to the second peak point $\varepsilon = 0.199$, $\sigma = 3.25$ GPa. As the strain increases, the stress–strain curve on the first platform in a relatively short (GH) fell to near M after stress.

3.1 Analysis of uniaxial tensile processes

Figure 3 shows the atomic structure evolution of the model in the I stage of uniaxial tensile deformation. The common neighbor atomic analysis in the OVITO software was used to color the atoms. In the initial deformation stage, the stress increased linearly as the strain increased. At this stage, the composite material was deformed elastically, and the atoms in the interface configuration were arranged neatly with almost no dislocation. As the strain increased further, as shown in Figure 3(b), dislocations began to nucleate at the heterogeneous interface between Cu and Al_2Cu, and activation of the microscopic deformation system was first observed in the Cu layer. When the strain increases to 0.072, the heteroboundary arches out the 1/6 ⟨112⟩ Shockley incomplete dislocation on the Cu side, and the dislocation moves along the {111} inside the Cu layer. At the same time, the dislocation starts nucleation at the heterointerface between Al and Al_2Cu. At a strain of 0.085 (Figure 3(a)) in the deformation stage of the peak stress, the heteroboundary arches out 1/6 ⟨112⟩ Shockley incomplete dislocation on the Al side. Due to the stress concentration at the heterogeneous interface, the dislocation nucleates at the interface and expands toward Cu and Al layers, which are prone to slip.

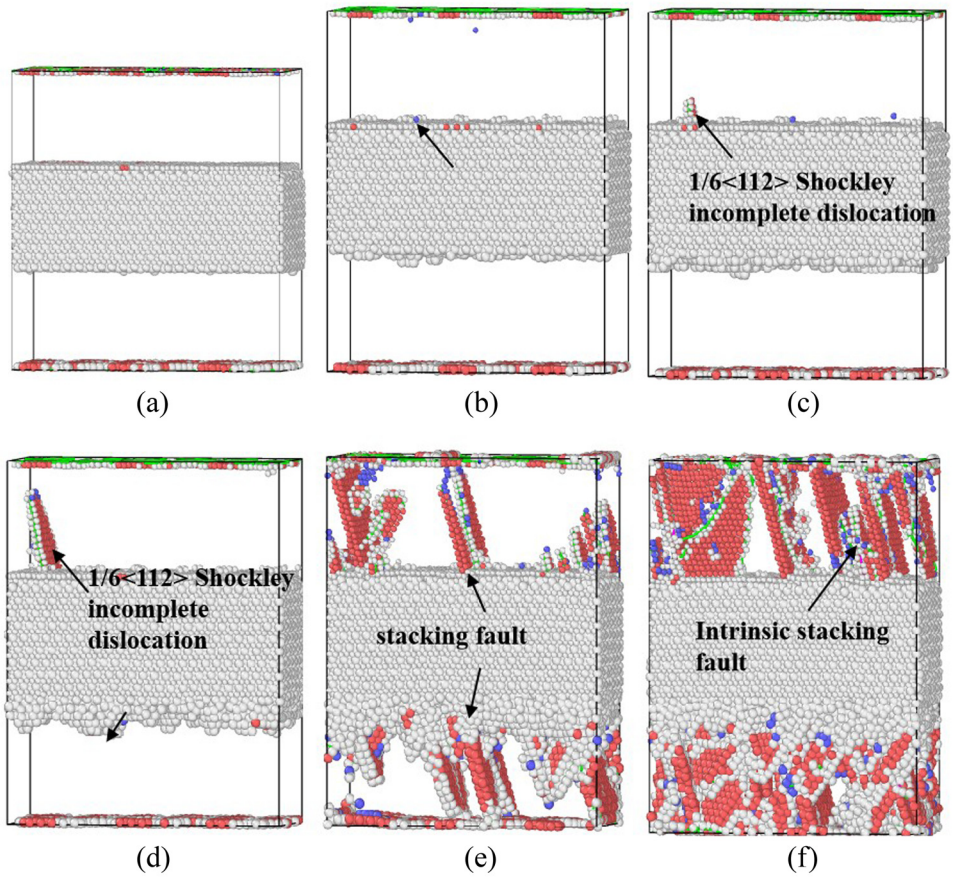

Figure 3: The Cu(111)/$Al_2Cu(\bar{1}10)$/Al(111) interface configuration corresponds to the mark point at the first stage in the tensile stress–strain curve (Figure 2). (a) $\varepsilon = 0$ (point A), (b) $\varepsilon = 0.068$ (point B), (c) $\varepsilon = 0.072$ (point C), (d) $\varepsilon = 0.085$ (point D), (e) $\varepsilon = 0.097$ (point E), (f) $\varepsilon = 0.107$ (point F).

The model then enters the plastic deformation stage. When the strain is 0.107, the 1/6 ⟨112⟩ Shockley incomplete dislocation penetrates the Cu and Al layers and leaves an insertion type dislocation (Figure 3(e)).

Figure 4 shows the atomic structure corresponding to each marked point of the stress–strain curve at the II stage of Cu(111)/$Al_2Cu(\bar{1}10)$/Al(111) interface configuration tensile deformation. Dislocation analysis (DXA, Figure 4(a)–(d)) and the CSP (Figure 4(e)–(h)) were used to color the atoms. The distribution of dislocation lines during stretching was evaluated by DXA. The green line is 1/6 ⟨112⟩ Shockley incomplete dislocation. As shown in Figure 4(a)–(d), as the strain increased, more 1/6 ⟨112⟩ Shockley partial dislocations were observed in the second stage. In the single Cu and Al layers, the dislocation disappeared from the free surface when the dislocation moved to the side surface (parallel to the plane of the tensile load). At this time, the 1/6 ⟨112⟩ Shockley incomplete dislocations formed in different directions produced several intersecting insertion-type stacking faults, and the overall stress of the model was released. When the strain reached 0.199, the number of irregularly arranged atoms at the interface increased significantly (Figure 4(f)). The atomic structure in the black ellipse indicates that cracks began to appear at the interface due to stress concentration. At this point, a variety of microscopic deformation systems interacted with the heterogeneous interface, which resulted in stress release and corresponded to a relatively short platform segment (GH segment) point appearing on the stress–strain curve in the second stage. When the strain was 0.3 (Figure 3(h)), the crack at the interface became more pronounced, and as the crack expanded, the stress concentration in the crack area increased, which made the stress of the entire model drop to near the M point until it fractured.

3.2 Model analysis at different strain rates

To study the effect of strain rate on multilayer tensile deformations, four different tensile simulation programs that corresponded to four different engineering strain

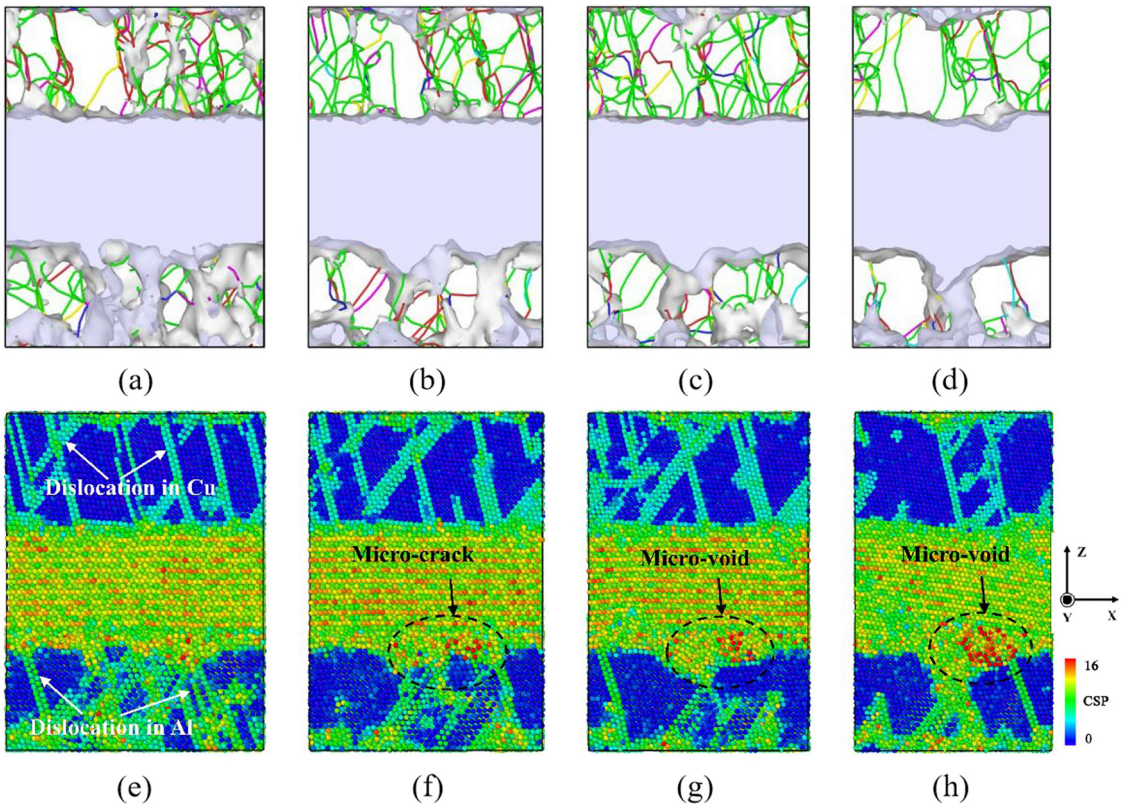

Figure 4: The Cu(111)/$Al_2Cu(\bar{1}10)$/Al(111) composite corresponding to the phase II mark in the tensile stress–strain curve: (a–d) DXA; (e–h) Centrosymmetric Parameter method (CSP). (a) ε = 0.123 (point F), (b) ε = 0.199 (point G), (c) ε = 0.029 (point H), (d) ε = 0.3 (point M), (e) ε = 0.123 (point F), (f) ε = 0.199 (point G) (g) ε = 0.229 (point H), (h) ε = 0.3 (point M).

rates were conducted. Programs using different strain rates needed different time steps so that the final strain of the entire is equaled to 0.30. Specific parameter settings are shown in Table 3. Their stress–strain curves at 300 K are shown in Figure 5.

For the tensile model of the vertical interface, the plastic deformation mechanism of the layered composites with different strain rates was also studied (Figure 5). According to those stress–strain curves, the mechanical behaviors of the models differed significantly under different strain rates. The stress increased linearly as the strain increased in the initial deformation stage, and the composite materials all underwent elastic deformation. The stress–strain curves at each strain rate were approximately coincident and had very similar slopes, which indicated the strain rate change had little effect

Table 3: Parameter settings under speed variables

Strain rate (ps^{-1})	Relaxation time (ps)	Step length (ps)	Temperature (K)	Time step
0.0005	50	0.001	300	600,000
0.001	50	0.001	300	300,000
0.005	50	0.001	300	60,000
0.01	50	0.001	300	30,000

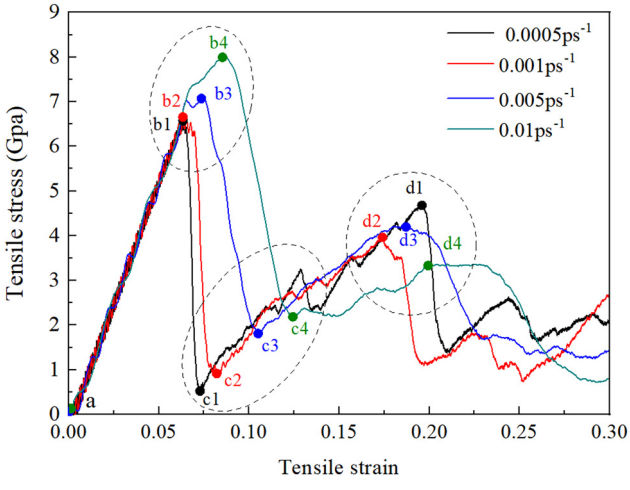

Figure 5: Stress–strain curves of different strain at 300 K.

on elastic deformation. In the range of simulated strain rate, the tensile strength of the composite showed a positive correlation to the engineering strain rate. When the strain rate was 0.0005 ps^{-1}, the curves decline rapidly, but that declined slowed as the strain rate increased.

On the one hand, face-centered cubic aluminum had higher strain rate sensitivity due to the number of dislocation movements. The strength of copper with low stacking fault energy was augmented by the formation of a lamellar twin structure [22]. On the other hand, as an intermediate transition phase between the copper and aluminum layers, the Al_2Cu layer has a good continuous structure. The Al_2Cu layer provides a good fracture transition during tensile deformation, so the overall structure of the model with different ductility deformed at the same time until it broke. Therefore, within the strain rate range, the tensile strength of the composite material increased with the strain rate increase.

Figure 6 shows the dislocation line distribution at the inflection point of the stress–strain curves at different strain rates, and DXA analyzed the dislocation line distribution during tensile. The green line represents the 1/6 ⟨112⟩ dislocation line, and the blue line represents the 1/2 ⟨110⟩ dislocation line. The exact dislocation line assigned

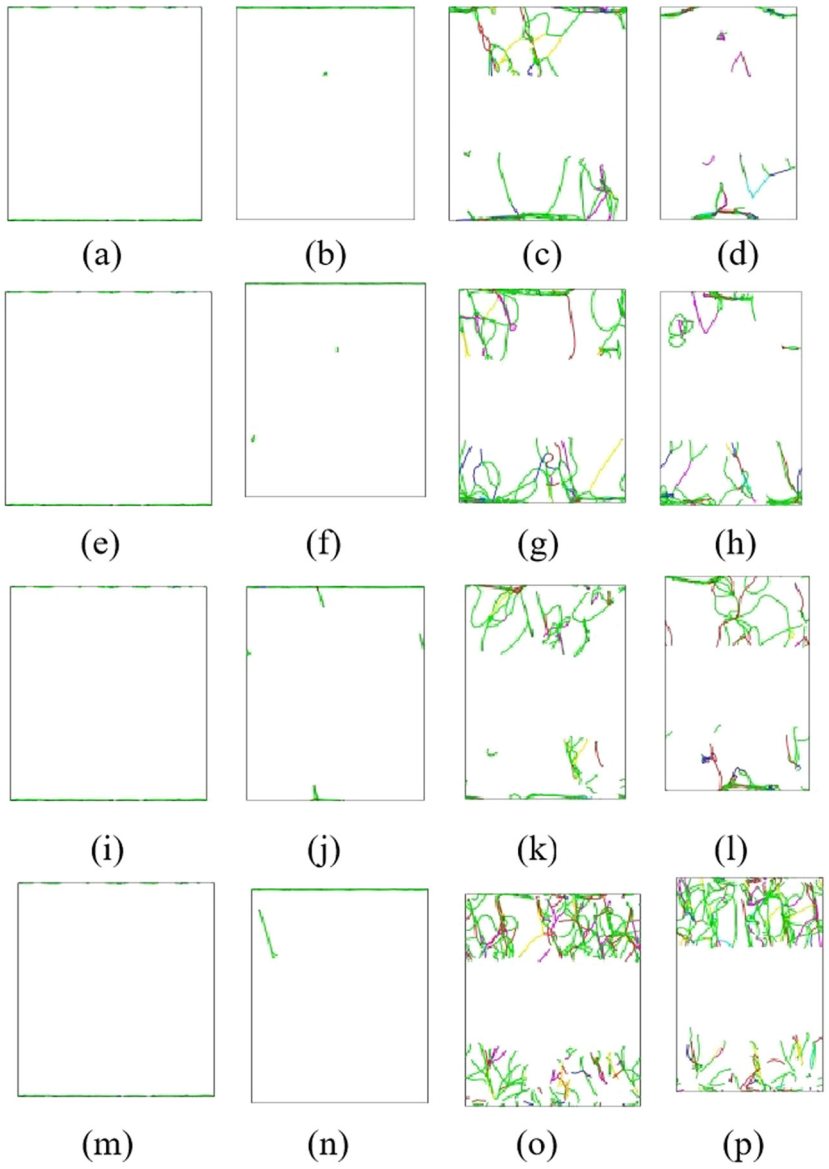

Figure 6: The distribution of the dislocation lines with respect to the marked points in the stress–strain curve (Figure 5). (a–d) 0.0005 ps^{-1}; (e)–(h) 0.001 ps^{-1}; (i–l) 0.005 ps^{-1}; and (m–p) 0.01 ps^{-1}. (a) point a1, (b) point b1, (c) point c1, (d) point d1, (e) point a2, (f) point b2, (g) point c2, (h) point d2, (i) point a3, (j) point b3, (k) point c3, (l) point d3, , (m) point a4, (n) point b4, (o) point c4, (p) point d4.

to the red line is uncertain. In the unstretched state, no dislocation lines were generated in the interface model (Figure 6(a), (e), (i), and (m)).

At a low strain rate, as the strain increases, the malposition in the composite body first occurs at point b (Figure 6(b) and (f)) and then maximizes at point c. On the one hand, the strength of the material plateaus at the yield stage when dislocations first occur. As the number of dislocation lines increases, the internal defects of the material increase, and the strength of the composite decreases. On the other hand, as the density of dislocations increases, the probability of simultaneous activation of dislocations in one direction decreases, and the mutual influence and staggering between dislocations make it difficult to move. This results in dislocation pinning, and the strength increases (Figure 5c and d segment).

Under different strain rates, the strength is independent of the strain rate in the initial strain stage. Strain rate hardening occurs when dislocations appear and the density of dislocations increases. The strength of the material increases as the strain rate increases and is consistent with literature reports [22–24].

3.3 Influence of temperature on tensile deformation

To study the influence of the temperature on the tensile deformation mechanical properties of Cu(111)/$Al_2Cu(\bar{1}10)$/Al(111), four temperatures (100, 300, 500, and 700 K) were chosen for simulation, while the other simulation parameter settings remained unchanged. The simulation system used isothermal and pressure system traces (NPT), and the stretching process took 40,000 steps.

Figure 7 shows the stress–strain curves at different temperatures. The curves for all four temperatures showed similar trends; the deformation mechanism remained significantly unchanged from 100 to 700 K. Figure 8 shows the ultimate tensile strength at different temperatures. Higher temperatures resulted in a smaller ultimate stretch. This shows that temperature had almost no effect on Young's modulus of the composite material, but the tensile strength and yield strain of the material gradually decreased at a higher temperature. Figure 9 shows the local strain distribution of the Cu(111)/$Al_2Cu(\bar{1}10)$/Al(111) interface model when the strain was 0.11. The local plastic deformation at high temperatures was more significant. This was produced by atomic thermal motion, which

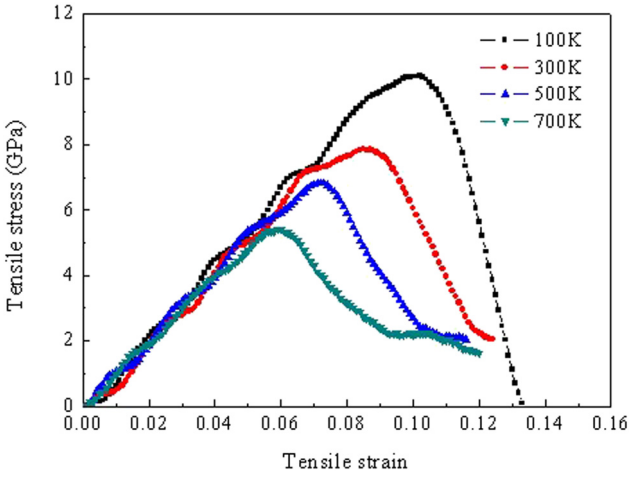

Figure 7: Stress–strain curves of the Cu(111)/$Al_2Cu(\bar{1}10)$/Al(111) model at different temperatures.

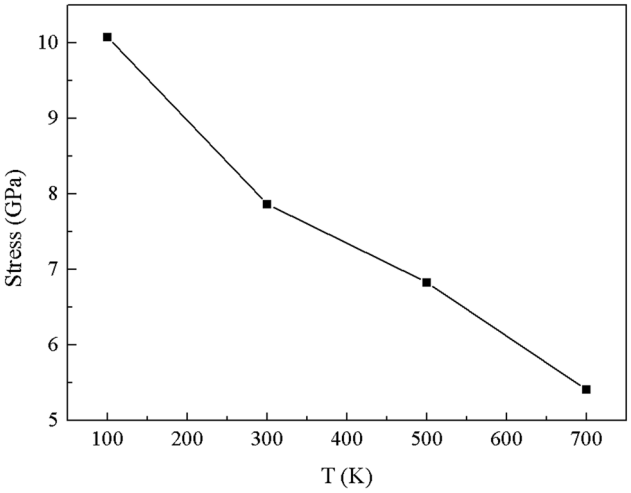

Figure 8: Ultimate tensile strength curves at different temperatures.

caused the composite material to soften and lose its mechanical characteristics as the temperature increased.

Figure 9 displays the evolution of the atomic configurations of the interface model at different temperatures. At 500 K and 700 K, the atoms existed in thermally activated states, as shown in Figure 9(c) and (d). With temperature increase, some point defects were observed in the initial unstressed state, and as the strain increased, the number of point defects also increased, leading to the formation of microcracks. At the same time, the increase in temperature increased the amount of activated movable dislocations. Consequently, high-density dislocations hindered the growth of microcracks and increased the deformation resistance of the material, thus decreasing the plasticity of the material. This decrease in plasticity

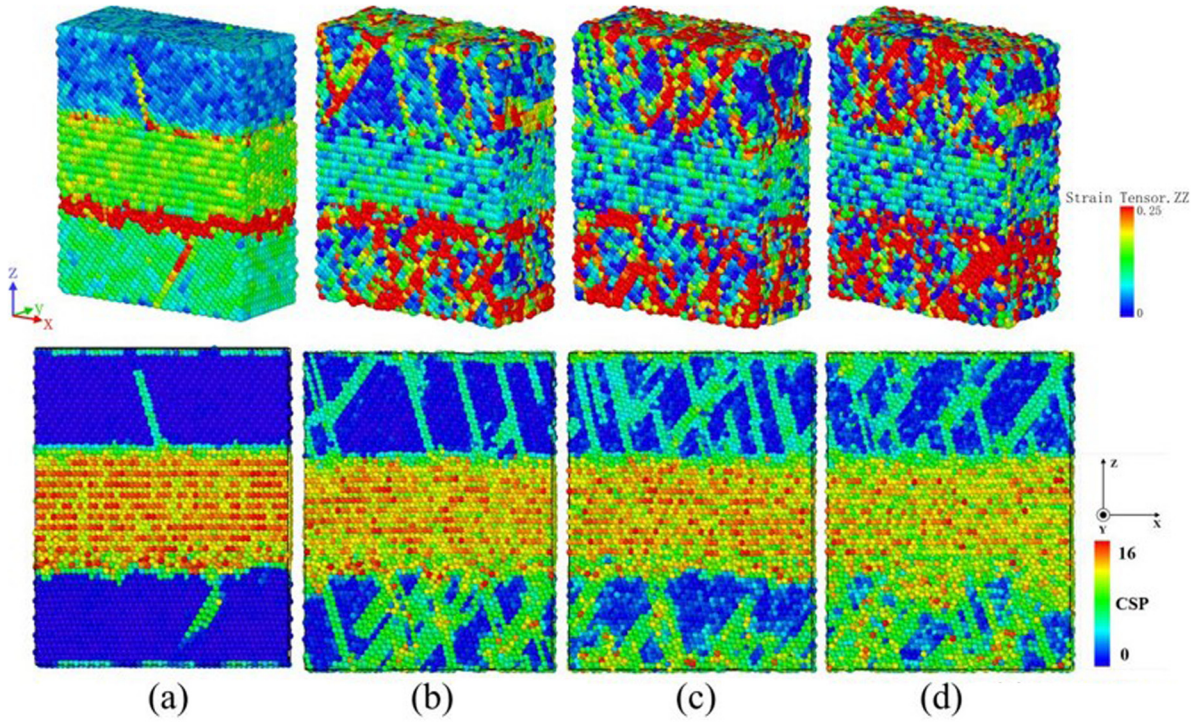

Figure 9: The distribution of the local plastic deformation and evolution of atomic configuration of the Cu(111)/$Al_2Cu(\bar{1}10)$/Al(111) interface model at a strain of 0.11. (a) 100 K, (b) 300 K, (c) 500 K, and (d) 700 K.

allows high-temperature conditions to promote dislocation nucleation.

4 Conclusion

The molecular dynamics simulations of uniaxial stretching of nano-layered Cu/Al composites containing brittle phase Al_2Cu were studied. The effects of temperature and strain rate on the tensile deformation of the system were studied in-depth, as well as the Al/Al_2Cu/Cu interface reaction. The following conclusions were drawn:

1) Under the tensile load of the Cu/Al_2Cu/Al interface, dislocations preferentially nucleated at the Cu/Al_2Cu heterogeneous interface and moved along the {111} crystal plane inside the Cu layer. The deformation mechanism was constrained slip within the layer. During this deformation, no initiation of plastic deformation occurred in the Al_2Cu layer.
2) The presence of the Al_2Cu layer made the overall structure deform at the same time, despite differences in strength and ductility.
3) The deformation mechanism remained basically unchanged from 100 to 700 K. Temperature has almost no effect on Young's modulus of the composite material; however, as the temperature increased, the tensile strength and yield strain of the material gradually declined.

Funding information: This research has been supported by the China's National Key R&D Program during the 14th five-year plan period (Grant No. 2021YFB3701304).

Author contributions: All authors have accepted responsibility for the entire content of this manuscript and approved its submission.

Conflict of interest: Authors state no conflict of interest.

References

[1] Liu G, Wang Q, Shang Z, Luo L, Ye B, Jiang H, et al. An investigation on microstructures and mechanical properties of ultra-low Cu layer thickness ratio Cu/8011/1060 clads. Metall Mater Trans A. 2019;50(12):5866–76.
[2] Liu T, Wang Q, Sui Y, Wang Q, Ding W. An investigation into interface formation and mechanical properties of aluminum-copper bimetal by squeeze casting. Mater Des. 2016;89:1137–46.

[3] Sheng LY, Yang F, Xi TF, Lai C, Ye HQ. Influence of heat treatment on interface of Cu/Al bimetal composite fabricated by cold rolling. Compos Part B. 2011;42(6):1468–73.
[4] Liu GP, Wang QD, Zhang L, Ye B, Jiang HY, Ding WJ. Effect of cooling rate on the microstructure and mechanical properties of Cu/Al bimetal fabricated by compound casting. Metall Mater Trans A. 2018;49(2):661–72.
[5] Jin T, Li G, Cao Y, Xu R, Shao S, Yang B. Experimental research on applying the copper-clad aluminum tube as connecting tubes of air conditioners. Energy Build. 2015;97:1–5.
[6] Manesh HD, Taheri AK. The effect of annealing treatment on mechanical properties of aluminum clad steel sheet. Mater Des. 2003;24(8):617–22.
[7] Kim WN, Hong SI. Interactive deformation and enhanced ductility of tri-layered Cu/Al/Cu clad composite. Mater Sci Eng A. 2016;651:976–86.
[8] Liu S, Wang A, Tian H, Xie J. The synergetic tensile deformation behavior of Cu/Al laminated composites prepared by twin-roll casting technology. Mater Res Express. 2019;6(1):016530.
[9] Liu SY, Wang AQ, Lu SJ, Xie JP. High-performance Cu/Al laminated composites fabricated by horizontal twin-roll casting. Materialwiss Werkstofftech. 2018;49(10):1213–23.
[10] Hug E, Bellido N. Brittleness study of intermetallic (Cu, Al) layers in copper-clad aluminium thin wires. Mater Sci Eng A. 2011;528(22–23):22–3.
[11] Xu B, Tong WP, Liu CZ, Zhang H, Zuo L, He JC. Effect of high magnetic field on growth behavior of compound layers during reactive diffusion between solid Cu and liquid Al. J Mater Sci Technol. 2011;27(9):856–60.
[12] Han Y, Ben L, Yao J, Wu C. Microstructural characterization of Cu/Al composites and effect of cooling rate at the Cu/Al interfacial region. Int J Miner Metall Mater. 2015;22(1):94–101.
[13] Rezaei R. Tensile mechanical characteristics and deformation mechanism of metal-graphene nanolayered composites. Comput Mater Sci. 2018;151:181–8.
[14] Yang W, Ayoub G, Salehinia I, Mansoor B, Zbib H. Deformation mechanisms in Ti/TiN multilayer under compressive loading. Acta Mater. 2017;122:99–108.
[15] Zhou Q, Li S, Huang P, Xu KW, Wang F, Lu TJ. Strengthening mechanism of super-hard nanoscale Cu/Al multilayers with negative enthalpy of mixing. APL Mater. 2016;4(9):096102.
[16] Weng S, Ning H, Fu T, Hu N, Zhao Y, Huang C, et al. Molecular dynamics study of strengthening mechanism of nanolaminated graphene/Cu composites under compression. Sci Rep. 2018;8(1):3089.
[17] Xu H, Liu C, Silberschmidt VV, Pramana SS, White TJ, Chen Z, et al. Behavior of aluminum oxide, intermetallics and voids in Cu–Al wire bonds. Acta Mater. 2011;59(14):5661–73.
[18] Gao K, Li S, Xu L, Fu H. Effect of sample size on intermetallic Al_2Cu microstructure and orientation evolution during directional solidification. J Cryst Growth. 2014;394:89–96.
[19] Shin D, Shyam A, Lee S, Yamamoto Y, Haynes JA. Solute segregation at the Al/θ′–Al_2Cu interface in Al–Cu alloys. Acta Mater. 2017;141:327–40.
[20] Zhou Q, Jian W, Misra A, Ping H, Xu K. Atomistic study of fundamental character and motion of dislocationsin intermetallic Al_2Cu. Int J Plast. 2016;87:100–13.
[21] Zhou XW, Ward DK, Foster ME. An analytical bond-order potential for the aluminum copper binary system. J Alloys Compd. 2016;680:752–67.
[22] Li X, Zu G, Wang P. Effect of strain rate on tensile performance of Al/Cu/Al laminated composites produced by asymmetrical roll bonding. Mater Sci Eng A. 2013;575:61–4.
[23] Fan H, Wang Q, El-Awady JA, Raabe D, Zaiser M. Strain rate dependency of dislocation plasticity. Nat Commun. 2020;12:1845.
[24] Niu JJ, Zhang JY, Liu G, Zhang P, Lei SY, Zhang GJ, et al. Size-dependent deformation mechanisms and strain-rate sensitivity in nanostructured Cu/X (X = Cr, Zr) multilayer films. Acta Mater. 2012;60(9):3677–89.